Applied Catalysis B: Environmental 197 (2016) 95–104

Contents lists available at ScienceDirect

Applied Catalysis B: Environmental

journal homepage: www.elsevier.com/locate/apcatb

Synergic effect of $Cu/Ce_{0.5}Pr_{0.5}O_{2-\delta}$ and $Ce_{0.5}Pr_{0.5}O_{2-\delta}$ in soot combustion

Verónica Rico-Pérez [a], Eleonora Aneggi [a,*], Agustín Bueno-López [b], Alessandro Trovarelli [a]

[a] Università di Udine, Dipartimento Politecnico di Ingegneria e Architettura, via del Cotonificio 108, 33100 Udine Italy
[b] University of Alicante, Department of Inorganic Chemistry, Carretera de San Vicente del Raspeig, 03690, Spain

ARTICLE INFO

Article history:
Received 17 December 2015
Received in revised form 11 February 2016
Accepted 24 February 2016
Available online 26 February 2016

Keywords:
Soot oxidation
Ceria
Praseodymium oxide
NO oxidation
CeO_2

ABSTRACT

A series of $5\%Cu/Ce_{0.5}Pr_{0.5}O_{2-\delta}$ and $Ce_{0.5}Pr_{0.5}O_{2-\delta}$ mixed oxides have been prepared and combined in different ratios. The resulting catalysts have been characterized by N_2 adsorption, XRD, Raman spectroscopy and H_2-TPR and tested for soot combustion by means of temperature-programmed experiments. The optimum catalyst for soot combustion in $NO_x/O_2/N_2$ atmosphere is the mixture containing 40% $Cu/Ce_{0.5}Pr_{0.5}O_{2-\delta}$ and 60% $Ce_{0.5}Pr_{0.5}O_{2-\delta}$. This mixture is more active than a reference catalyst containing the same amount of copper distributed in the whole Ce-Pr mixed oxide support. The benefit of mixing $Ce_{0.5}Pr_{0.5}O_{2-\delta}$ particles with and without copper in a single catalyst formulation is that the participation of the two soot combustion mechanisms based on active oxygen and NO_2, respectively, is optimized. The particles with copper mainly promote the catalytic oxidation of NO to NO_2 (the NO_x-assisted mechanism) while those without copper are more effective in promoting the active oxygen mechanism. If copper is loaded homogeneously in all the $Ce_{0.5}Pr_{0.5}O_{2-\delta}$ particles, the positive effect of copper improving NO_2 production is offset by the lower efficiency of the active oxygen mechanism, due to a lack of active oxygen on the $Ce_{0.5}Pr_{0.5}O_{2-\delta}$ support.

1. Introduction

Health and environmental problems are the reasons for the important concern about the removal of soot particles emitted from diesel engine [1,2]. Filtering in a DPF (Diesel Particulate Filter) followed by combustion is one of the most promising technologies for soot abatement. Since the onset temperature for soot combustion is too high for spontaneous regeneration of the filters, it is necessary to ignite soot periodically by raising the temperature with or without diesel fuel addition [3,4] and catalysts are required to promote filter regeneration.

Several different catalysts have been studied for soot combustion [5], and formulations containing ceria-based materials are among the most promising; however, thermal stability of bare ceria is rather poor and ceria undergoes rapid sintering at high temperatures, which adversely affect its catalytic properties [6–8]. Therefore, modification of ceria is necessary in order to improve the stability towards sintering and the oxidation activity of the resulting catalysts. An approach to boost the catalytic activity is the preparation of materials with appropriate morphologies that can provide a large number of soot-catalyst contact points and that can expose more reactive planes enhancing the oxygen release capacity [9–11]. Improved thermal stability and changes in the physicochemical properties of ceria are also obtained by introducing other metal ions into the ceria structure, which may change the redox properties and may favour the creation of the oxygen vacancies improving the oxygen mobility through the catalyst [12–17]. The most promising doped-ceria active phases seem to be those containing Pr, Zr or La as main dopant [18–26], where the optimum loading depends on the dopant size and on the resulting redox properties [27].

The catalytic combustion of soot promoted by ceria-based catalysts takes place through two different reaction mechanisms, which are usually referred to as the active oxygen mechanism and the NO_x-assisted mechanism [27]. In the active oxygen mechanism, ceria exchanges its oxygen with gas-phase O_2 creating highly reactive oxygen species (the so-called "active oxygen"), and active oxygen oxidizes soot very efficiently. Some authors have related these active oxygen species with the formation of superoxides and peroxides on the ceria surface [28,29]. They could form via oxygen adsorption on the reduced surface of ceria in the vicinity of soot and then they react with carbon forming CO_2. On the soot/ceria interface, soot can reduce ceria initiating the "active oxygen" route that can promote the oxidation by a spillover mechanism. The main

* Corresponding author.
E-mail address: eleonora.aneggi@uniud.it (E. Aneggi).

http://dx.doi.org/10.1016/j.apcatb.2016.02.051
0926-3373/

Table 1
Composition of catalyst formulations investigated.

Sample name	Catalyst composition (wt.%)	
	(5%)Cu/$Ce_{0.5}Pr_{0.5}O_{2-\delta}$	$Ce_{0.5}Pr_{0.5}O_{2-\delta}$
CePr	0	100
20CuCePr + 80CePr	20	80
40CuCePr + 60CePr	40	60
60CuCePr + 40CePr	60	40
80CuCePr + 20CePr	80	20
CuCePr	100	0
(2%)CuCePr	(2%)Cu/$Ce_{0.5}Pr_{0.5}O_{2-\delta}$	0

limitation of this reaction pathway is the short lifetime of the active oxygen species, which must be able to reach the soot particles. In a real DPF, the solid–solid contact between soot and catalyst particles is limited to few contact points and this hinders the transfer of active oxygen from ceria to soot. The other pathway, the so-called NO_x-assisted mechanism, involves the catalytic oxidation of NO to NO_2, which is more oxidizing than NO and O_2 and successfully initiates soot combustion [1,27,30–35]. This is the basis of the so-called continuously regenerating trap (CRT) developed by Johnson Matthey [36], where a Pt catalyst accelerates NO oxidation. It has been reported that the NO oxidation capacity of ceria-based oxides can be improved by impregnation of transition metals, like copper, and this would be interesting to develop noble metal-free soot combustion catalysts [37,38]. Comparing the two ceria-catalysed soot combustion mechanisms, the main advantage of the NO_x-assisted mechanism is that NO_2 is stable and does not have lifetime restrictions to move from the catalyst to soot particles. However, the intrinsic reactivity of active oxygen is believed to be much higher than that of NO_2 [39].

In this study we investigate in detail soot oxidation activity over a series of Cu loaded $Ce_{0.5}Pr_{0.5}O_{2-\delta}$ catalysts with different amount of copper. The catalysts have been prepared by mixing Cu/$Ce_{0.5}Pr_{0.5}O_{2-\delta}$ with $Ce_{0.5}Pr_{0.5}O_{2-\delta}$ in appropriate amount in order to obtain increasing Cu content. Considering previous investigations [23], the $Ce_{0.5}Pr_{0.5}O_{2-\delta}$ mixed oxide has been selected for this study as optimized ceria-based soot combustion catalyst, and copper has been selected as transition metal to improve the NO oxidation capacity. The aim of the study is to demonstrate that the design of soot combustion ceria-based catalysts can be improved in formulations that contain a combination of ceria particles with and without copper in order to optimize the simultaneous and synergic contribution of the two oxidation mechanisms (active oxygen and NO_x assisted) to the overall combustion reaction.

2. Experimental

2.1. Catalyst preparation

$Ce_{0.5}Pr_{0.5}O_{2-\delta}$ was prepared by mixing in an agate mortar the proper amounts of cerium nitrate (Treibacher Industrie) and praseodymium nitrate (Sigma-Aldrich) followed by calcination at 500 °C for 3 h 5 wt.% Cu was deposited over $Ce_{0.5}Pr_{0.5}O_{2-\delta}$ by incipient wetness impregnation of $Ce_{0.5}Pr_{0.5}O_{2-\delta}$ with the appropriated amount of $Cu(NO_3)_2{\cdot}2.5H_2O$ (98%, Sigma-Aldrich). Finally, it was dried overnight at 100 °C and calcined at 500 °C for 3 h.

The investigated catalysts were obtained by mixing proper amounts of $Ce_{0.5}Pr_{0.5}O_{2-\delta}$ and 5%Cu/$Ce_{0.5}Pr_{0.5}O_{2-\delta}$ with a spatula in different weight ratios. The resulting mixtures will be referred to as xCuCePr + yCePr, where x and y indicate the weight percentage of 5%Cu/$Ce_{0.5}Pr_{0.5}O_{2-\delta}$ and $Ce_{0.5}Pr_{0.5}O_{2-\delta}$ in the mixture, respectively (see Table 1).

For comparison, an additional catalyst with 2% of copper (2%Cu/$Ce_{0.5}Pr_{0.5}O_{2-\delta}$) was prepared by incipient wetness impregnation of $Ce_{0.5}Pr_{0.5}O_{2-\delta}$ with the copper precursor following the previously described impregnation and calcination procedures. This reference catalyst will be referred to as (2%)CuCePr. The characteristics of all catalysts are summarized in Table 2.

Table 2
Main characteristics of catalysts investigated.

Sample	Cu[a] (wt.%)	BET surface area (m^2/g)	Lattice parameter (Å)[b]	Particle size (nm)
CePr	0	24	5.4147(3)	12
20CuCePr + 80CePr	1	27	5.4143(3)	12
40CuCePr + 60CePr	2	26	5.4127(3)	12
60CuCePr + 40CePr	3	26	5.4126(3)	12
80CuCePr + 20CePr	4	30	5.4117(1)	12
CuCePr	5	26	5.4116(3)	12
(2%)CuCePr	2	26	5.4141(3)	12

[a] nominal copper loading.
[b] Lattice parameter calculated with Rietveld refinement for a cubic structure.

2.2. Catalysts characterization

Textural properties of all catalysts were studied by nitrogen adsorption at −196 °C, using a Tristar 3000 gas adsorption analyser (Micromeritics). Structural features of the catalysts were characterized by X-ray diffraction (XRD). XRD patterns were recorded on a Philips X'Pert diffractometer operated at 40 kV and 40 mA using nickel-filtered Cu-Kα radiation. Diffractograms were collected using a step size of 0.02° and a counting time of 40 s per angular abscissa in the range 20–80°. The Philips X'Pert HighScore software was used for phase identification. The mean crystallite size was estimated from the full width at the half maximum (FWHM) of the X-ray diffraction peak using the Scherrer equation [40] with a correction for instrument line broadening. Rietveld refinement [41] of XRD pattern was performed by means of GSAS-EXPGUI program [42,43].

Raman spectra were recorded in a Jobin Yvon Horiba Raman dispersive spectrometer with a variable-power He-Ne laser source (632.8 nm) and 1 mW laser power, using a confocal microscope. The laser approached the sample using an Olympus 10× lens. The spectra were acquired after 2 scan of 120 s each one.

The reducibility of the catalysts was studied by temperature-programmed reduction (TPR) experiments; catalysts (50 mg) were heated at a constant rate (10 °C/min) in a U-shaped quartz reactor from room temperature to 500 °C under a flowing hydrogen/nitrogen mixture (35 ml/min, 4.5% H_2 in N_2). The hydrogen consumption was monitored using a thermal conductivity detector (TCD). Quantification of H_2 consumption was carried out by calibrating the signal with the introduction of known amounts of hydrogen.

2.3. Catalytic activity

Samples for catalytic measurements were prepared by mixing accurately each catalyst with soot (Printex-U by Degussa AG) in tight and loose contact mode. The former was achieved by mixing a soot/catalyst (1/20 wt ratio) in an agate mortar for 10 min, while loose contact samples were obtained by mixing soot/catalyst (1/4 wt ratio) for 2 min with a spatula. Soot oxidation for samples mixed under tight contact conditions was tested by running TGA experiments (Q500, TA Instruments) under O_2/N_2. The soot-catalyst sample (ca. 10 mg) was placed in a small flat Pt crucible licked by an air flow (60 ml/min) tangent to the sample, and heated at a constant rate (10 °C/min) up to 800 °C. Before the catalytic tests the samples were subjected to a 1 h pre-treatment at 150 °C under inert atmosphere in order to eliminate the adsorbed water. As a

measure of activity, the temperature at which 50% of weight loss is observed (T50, corresponding to removal of 50% of soot) was used.

Reaction rate measurements were also performed by isothermal experiments; ca. 20 mg of a catalyst–soot mixture were pre-treated for 1 h at 150 °C under nitrogen atmosphere. Then they were heated at a constant rate (10 °C/min) up to the reaction temperature (350 °C) followed by switching to air. The reaction was followed for 1 h using the weight loss rate as a measure of soot oxidation rate. Specific reaction rate has been normalized to the soot initially present in the reactor and to the catalyst weight $\mu g_{soot}/(g_{sootinitial} \cdot s \cdot g_{catalyst})$. The reaction rate was calculated at 5% of conversion [9,22].

The soot combustion activity for samples mixed in loose contact mode was determined by temperature programmed oxidation (TPO) experiments under $NO/O_2/N_2$ mixtures. The catalytic tests were performed in a quartz reactor coupled to FT-IR gas analysers (MultiGas 2030, MKS) by monitoring the concentrations of CO_2, CO, NO_2 and NO at the outlet of the reactor. During the TPO experiments 20 mg of mixture were heated at a constant rate (10 °C/min), while the gas flow (500 ppm NO/10% O_2/N_2) was kept fixed at ca. 500 ml/min. The catalyst temperature was checked by a chromel–alumel thermocouple, located on the catalyst bed. As a measure of activity, the temperature at which 50% of conversion is observed (T50) was used. The onset temperature for soot combustion is also evaluated with the temperature of 5% conversion (T5). Reproducibility of results was verified by running several experiments on similar samples and the results in terms of T50 were always within ±3 °C.

TPO experiments under $NO/O_2/N_2$ atmosphere were also performed only with the catalysts (without soot) in order to evaluate their NO oxidation capacity, and the temperature of the maximum production of NO_2 (Tm) was used as an indication of activity. Reaction rate for NO oxidation were also determined at low conversion by assuming differential reactor conditions (i.e., conv. <10%).

3. Results

3.1. Textural and structural characterization

Fig. 1 displays X-ray diffractograms of the catalysts. They show characteristic signals corresponding to reflections of the planes (1 1 1), (2 0 0), (2 2 0), (3 1 1) and (2 2 2) of the fluorite structure. Other two weak peaks assigned to CuO were also detected at $2\theta = 35.5$ and 38.6° for the samples with the higher amount of copper. Cell parameters estimated for the ceria-praseodymia solid solution are slightly higher than that of pure ceria (5.4110 Å vs 5.4147 Å) indicating that the majority of Pr is included in solid solution as Pr^{4+} cation whose ionic radius is similar to that of Ce^{4+}. According to the Vegard low [44,45], the slight increase of the cell parameter is compatible with the presence of some Pr^{3+} (ca. 3%) inside the structure. Parameters for copper-containing catalysts are only slightly lower than that of the copper free sample (Table 2). This suggests that the majority of copper remains on the surface, and that is not significantly incorporated into the fluorite structure, in agreement with other literature works [37,46]. Also, no evidence of segregation of pure praseodymium oxide phase was revealed by XRD.

Evaluation of BET calculated from N_2 adsorption isotherms reveals that no significant difference exists among catalysts. The values of BET surface area are located in the range 24–30 m^2/g for all mixtures (Table 2). This is in agreement with the crystallite sizes of 12 nm that were obtained for all catalysts.

Fig. 2 shows the Raman spectra of the investigated materials. The spectra evidenced two sharp bands at ca. 440 and 570 cm^{-1} and two broad bands at 185 and 1120 cm^{-1}. Raman spectra of ceria reported in literature [47] exhibit a single sharp band at around 465 cm^{-1} which is ascribed to the Raman active F_{2g} mode of CeO_2, characteristic of a fluorite structured material. This can be viewed as a symmetric breathing mode of the oxygen atoms surrounding each cation. Since only the oxygen atoms move, the mode frequency should be nearly independent of the cation mass. Luo et al. [48] observed that the bands at 465 and 1170 cm^{-1} (ascribed to CeO_2) underwent a systematic shift to lower frequencies with the increasing of Pr content, indicating that the incorporation of Pr into the ceria lattice results in the formation of the solid solution [23]. In agreement with these results, in our catalysts the bands are shifted down to 440 and 1120 cm^{-1} suggesting the formation of ceria-praseodymia solid solution. The bands at 185 and 570 cm^{-1} are linked to oxygen vacancies in the CeO_2 lattice [49]; particularly, the band at 185 cm^{-1} may be ascribed to the asymmetric vibration caused by the formation of oxygen vacancies [48]. The reason for the formation of the Raman band at 570 cm^{-1} is that when two Ce^{4+} ions are substituted by two Pr^{3+} ions, one oxygen vacancy is introduced into the fluorite lattice in order to maintain the electric neutrality, which will cause the broad peak on the high frequency side of the F_{2g} band. Thus, the band at 570 cm^{-1} can be linked to lattice defects, which results in the creation of oxygen vacancies. In addition the peak at 185 cm^{-1} is correlated to the peak at 570 cm^{-1} [49,50], and could suggest a certain degree of tetragonalization of the fluorite lattice.

In conclusion, characterization of the catalysts obtained by means of N_2 adsorption, XRD and Raman spectroscopy reveals that all samples are homogeneous and characterized by similar textural and structural properties.

3.2. Catalysts reducibility

The reducibility of the catalysts has been studied by temperature-programmed reduction (H_2-TPR) experiments with H_2, Fig. 3. For the copper-free $Ce_{0.5}Pr_{0.5}O_{2-\delta}$ catalyst a single broad peak was found with an onset temperature of ca. 275 °C and centred at around 400 °C, in agreement with literature results [51,52]. The overall H_2 consumption calculated from the TPR profile is 1.72 mmol/g, well above the quantity necessary to reduce surface Ce^{4+} and Pr^{4+}. This suggests that surface and bulk Ce^{4+} and Pr^{4+} reduction occurs concurrently due to the good bulk oxygen mobility induced by the presence of praseodymium cations [51,53]. Thus, it is likely that the oxygen vacancies generated by the presence of praseodymium lead to an easier exchange of oxygen through reactive oxygen species that can be formed and are easily reduced by H_2 at low temperature [48]. On the other hand, the presence of copper modifies the redox behaviour of both CuO and ceria because of the metal-support interaction at the interface [54–56]. The reduction peaks are therefore shifted to lower temperatures compared to the reduction of the pure oxides (CuO or $Ce_{0.5}Pr_{0.5}O_{2-\delta}$). Fig. 3A shows that the broad reduction peak at ca. 400 °C (corresponding to $Ce_{0.5}Pr_{0.5}O_{2-\delta}$ reduction) is shifted to lower temperatures when increasing the fraction of CuCePr in the catalyst. In addition, a broad signal assigned to CuO reduction appears between 100 and 300 °C [52,57]. This peak is not observed on the copper-free CePr catalyst. Under similar experimental conditions, pure CuO profile exhibits a single reduction peak centred at ca. 320–380 °C [37,48,54,56], a temperature which is markedly higher than the temperatures of the reduction events of any of the catalysts tested in the present study, probing the synergic effect between copper and the support for reduction of the Cu^{2+}, $Ce^{4+}$and Pr^{4+} cations.

The quantitative analysis of the TPR profile (Table 3) reveals that the amount of H_2 consumed in the first peak exceeds that required for complete reduction of CuO to Cu, suggesting that part of Ce^{4+} and Pr^{4+} is reduced at low temperature (100–300 °C) through a spillover process promoted at the Cu O-$Ce_{0.5}Pr_{0.5}O_{2-\delta}$ interface [37,58].

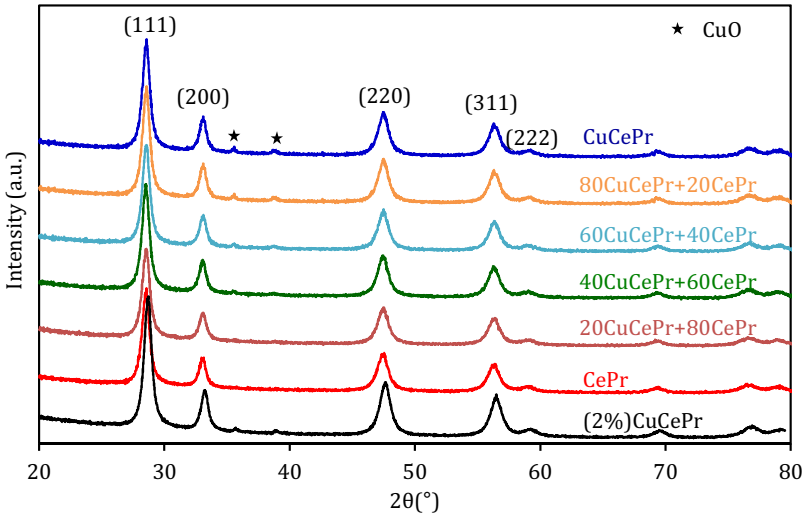

Fig. 1. Powder X-ray diffraction profiles of all samples.

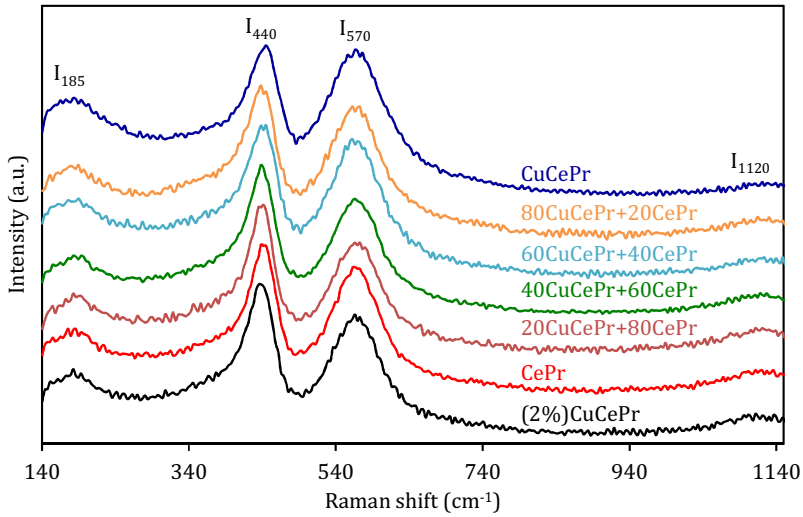

Fig. 2. Raman spectra of the catalysts.

Table 3
H_2-TPR and soot oxidation data.

sample	Calculated H_2 uptake[a] (mmol H_2/g_{cat})	H_2 uptake[b] (mmol H_2/g_{cat})	H_2/CuO	Total H_2 uptake[c] (mmol H_2/g_{cat})	T50[d] (°C)	Soot oxidation rate[e]
CePr	/	/	/	1.72	378	198
20CuCePr + 80CePr	0.16	0.62	3.94	1.61	377	187
40CuCePr + 60CePr	0.31	1.07	3.40	1.61	378	190
60CuCePr + 40CePr	0.47	1.53	3.24	1.79	376	175
80CuCePr + 20CePr	0.63	1.81	2.87	1.93	377	189
CuCePr	0.79	2.13	2.71	2.13	378	184
(2%)CuCePr	0.31	1.5	4.77	1.50	379	212

[a] Calculated hydrogen consumption for CuO reduction.
[b] H_2 consumed from the first peak.
[c] Overall H_2 consumption in H_2-TPR.
[d] Temperature of 50% conversion for soot oxidation under O_2/N_2 atmosphere.
[e] Rate of soot oxidation ($\mu g_{soot}/(g_{sootinitial} * s * g_{catalyst})$) measured at 350 °C for soot oxidation under O_2/N_2 atmosphere. Value to be multiplied by 100.

To summarize, in Fig. 3A two different reduction events can be identified. The one taking place at low temperature corresponds to the reduction of CuO species and surface Ce^{4+} and Pr^{4+} cations in close contact with copper. The other, located at temperature higher than 275 °C, corresponds to the reduction of the fraction of $Ce_{0.5}Pr_{0.5}O_{2-\delta}$ which is not in close contact with copper but still benefits from the presence of the transition metal. A boundary between

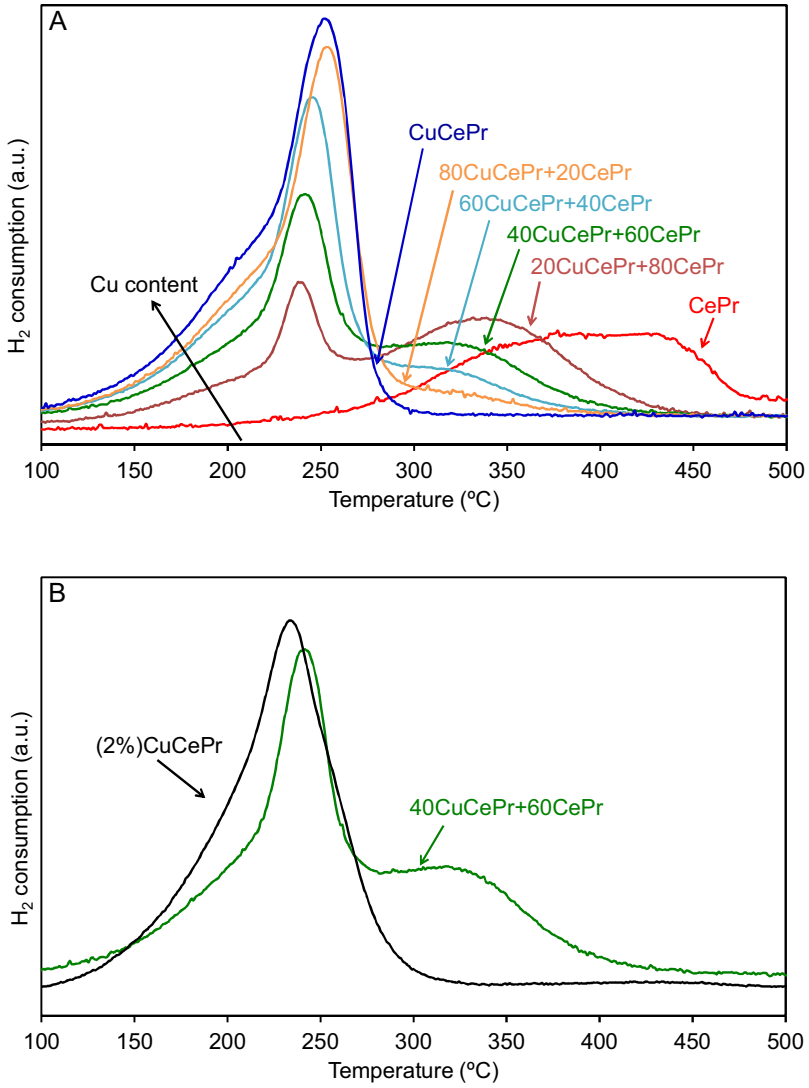

Fig. 3. (A) H_2-TPR profiles of investigated catalysts; (B) comparison of 40CuCePr + 60CePr and (2%)CuCePr.

the reduction of the physical mixture of CuCePr and CePr is detected at ca. 275 °C.

The presence of two different reduction events is highlighted by comparing the reduction profiles of 40CuCePr + 60CePr with that of the reference catalyst (2%)CuCePr in Fig. 3B. Note that the total amount of copper is the same on (2%)CuCePr and on 40CuCePr + 60CePr, but on the former catalyst copper is distributed over all $Ce_{0.5}Pr_{0.5}O_{2-\delta}$ particles while on the latter the same amount of copper is loaded only on 40% of the $Ce_{0.5}Pr_{0.5}O_{2-\delta}$ particles. The reduction profile of (2%)CuCePr exhibits a single reduction band correlated to the simultaneous reduction of Cu^{2+}, Ce^{4+} and Pr^{4+} cations while the physical mixture (40CuCePr + 60CePr) shows two signals due to the presence of different reduction paths. In the low temperature reduction peak Cu^{2+} is reduced together with Ce^{4+} and Pr^{4+} cations in close contact with copper, while in the high temperature reduction peak only Ce^{4+} and Pr^{4+} cations which are not in close contact with copper are reduced.

In conclusion, a two-step reduction profile is observed for all the xCuCePr + yCePr catalysts that contain copper, with peak temperatures considerably lower than those of pure CuO and $Ce_{0.5}Pr_{0.5}O_{2-\delta}$.

3.3. Catalytic tests

The evaluation of NO to NO_2 oxidation ability of the different catalysts was carried out by means of temperature-programmed oxidation experiments (Fig. 4). All the catalysts are active in NO oxidation with the onset of activity located at around 250–300 °C. Differences in NO conversion to NO_2 are only important before the thermodynamic equilibrium of the NO/NO_2 reaction (dotted line in Fig. 4A), and therefore the NO_2 production profiles are identical above ca. 450/500 °C. Reaction rate for NO_2 production was calculated at 285 °C for conversion lower than 10%. Fig. 4B revealed that the reaction rate increased almost linearly with the amount of CuCePr present in the sample, i.e. with the amount of copper, confirming the key role of copper to improve the NO oxidation capacity of the ceria-based oxides.

Soot oxidation was studied in O_2/N_2 atmosphere for tight contact mixtures and the results are reported in Table 3. The T50 values vary in a very narrow range (376–379 °C), indicating a similar catalytic activity for all the samples. Comparable results (not shown for the sake of clarity) were obtained also by TPO experiments. The oxidation rate values (Table 3) are also in agreement with the activity behaviour, confirming that the ability of catalysts to oxidize soot is

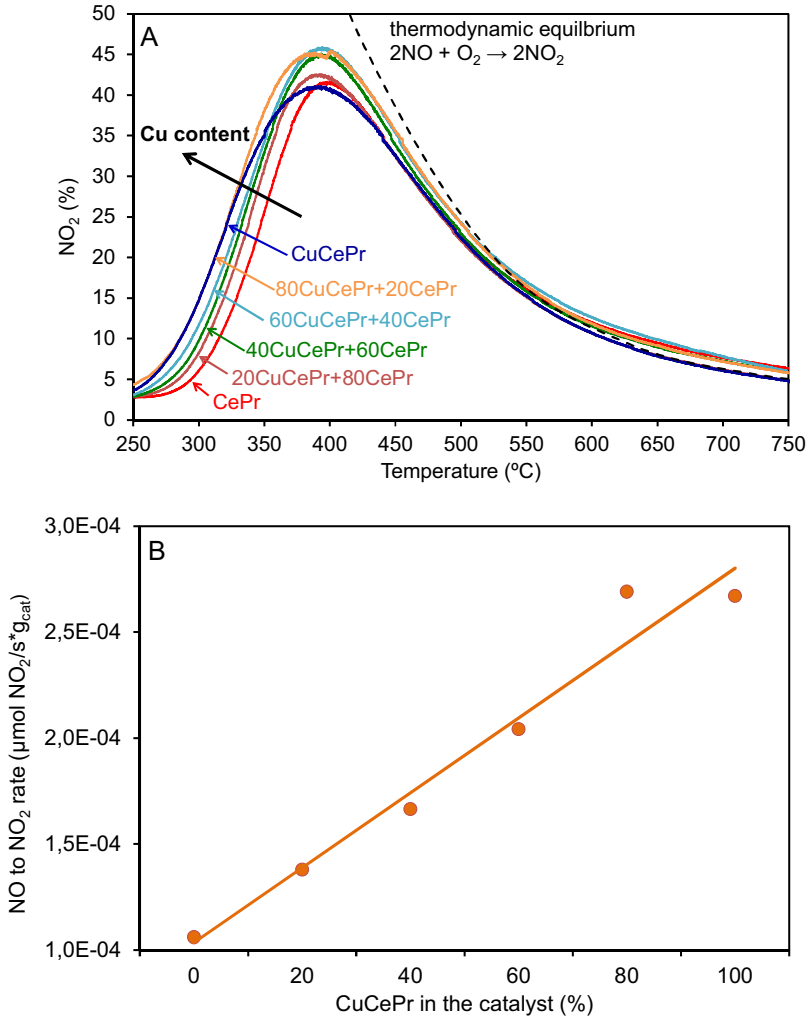

Fig. 4. (A) NO_2 production profiles in NO oxidation and (B) reaction rate calculated at 285 °C.

independent on copper content. These experiments point out that copper does not affect the combustion of soot by O_2 if the soot-ceria catalyst contact is tight; that is, if there are no restrictions for the active oxygen from ceria to be transferred to soot.

The T5 and T50 values extracted from TPO experiments under $NO/O_2/N_2$ with loose contact soot-catalyst mixtures are reported in Fig. 5. Soot oxidation activity under these conditions depends on catalyst composition. In both cases the 40CuCePr + 60CePr catalyst resulted to be the most active with the lowest T5 and T50; the activity curve has an almost inverse volcano-type profile with a minimum oxidation temperature in the middle composition range. This indicates that NO_x-assisted soot combustion mechanism is not the main combustion pathway, as in this case a linear dependence of the activity on the copper content should have been observed, with the catalyst with the higher amount of copper (CuCePr) being the most active in soot oxidation. It seems therefore that NO oxidation capacity alone cannot explain the order of activity and a combination of two different mechanisms should be considered to explain the behaviour.

The catalytic combustion of soot was also compared over two catalysts with the same copper content, (2%)CuCePr and 40CuCePr + 60CePr; the former with copper loaded in the whole $Ce_{0.5}Pr_{0.5}O_{2-\delta}$ support and the latter with copper loaded only in 40% of the $Ce_{0.5}Pr_{0.5}O_{2-\delta}$ support. Fig. 6 compiles conversion curves obtained in soot oxidation experiments with $NO/O_2/N_2$ and loose soot/catalyst mixtures with a soot/catalyst ratio of 1/4. The results revealed that the catalyst with two components is more active than that with copper loaded on the whole support.

4. Discussion

Characterization of the catalysts obtained by means of BET, XRD and Raman spectroscopy revealed that all catalysts have similar textural and structural properties, unaltered by the presence of copper. On the contrary, the reducibility of the xCuCePr + yCePr catalyst is significantly affected by copper, and two reduction processes were identified: the one occurring at lower temperature is attributed to Cu^{2+} reduction together with reduction of the Ce^{4+} and Pr^{4+} cations located near copper, the one occurring at higher temperature is assigned to reduction of Ce^{4+} and Pr^{4+} cations which are not in close contact with copper. The presence of two different reduction events can be associated to the presence of two different types of active sites in the mechanism of catalytic combustion of soot under $NO/O_2/N_2$ mixtures, which are summarized in Fig. 7. Fig. 7A describes the active oxygen mechanism; in this mechanism, the catalyst acts as a redox centre, transferring oxygen from gas-phase O_2 to soot, though an oxygen exchange process. The catalyst reduction is initiated at the contact/interface area between soot and catalyst, forming reduced sites that are reoxidized by gas phase O_2. The highly reactive oxygen species transferred from the catalyst to soot (the so-called “active oxygen”) can effectively oxidize the soot particles in direct contact with them. The soot in con-

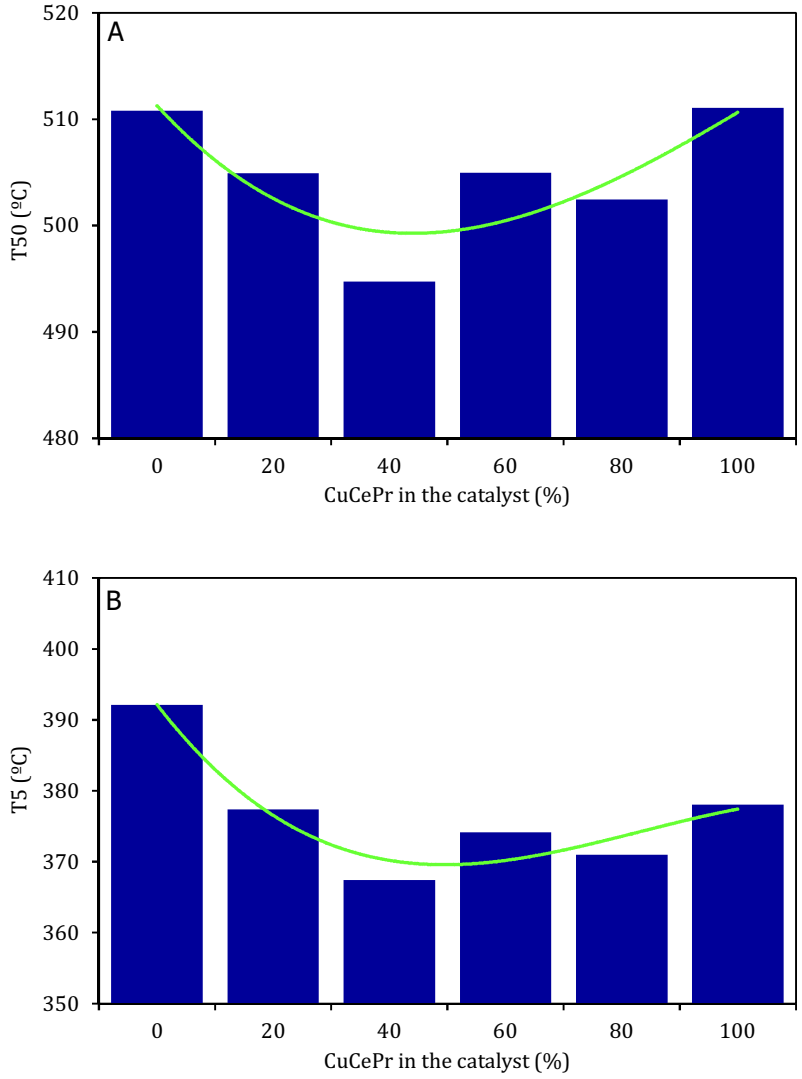

Fig. 5. (A) T50 and (B) T5 from TPO experiments carried out under 500 ppm NO/10%O_2/N_2 atmosphere.

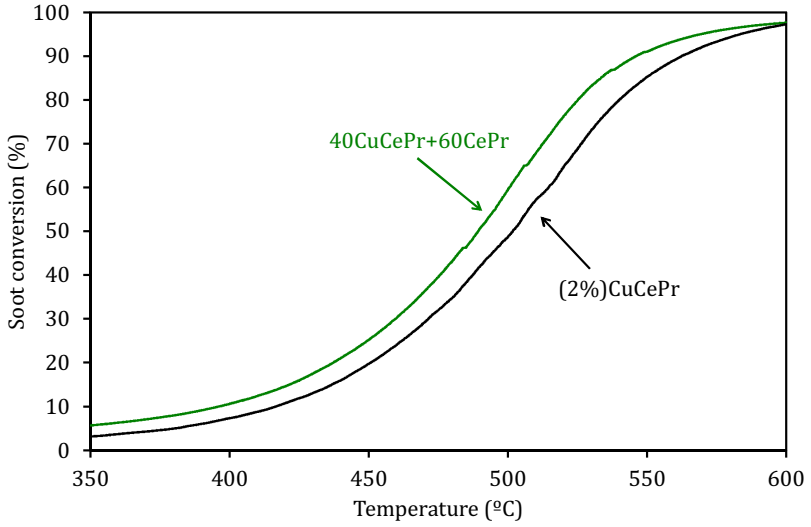

Fig. 6. Soot conversion profiles of catalysts with the same amount of copper: (2%)CuCePr (green) and 40CuCePr + 60CePr (black). (For interpretation of the references to color in this figure legend, the reader is referred to the web version of this article.)

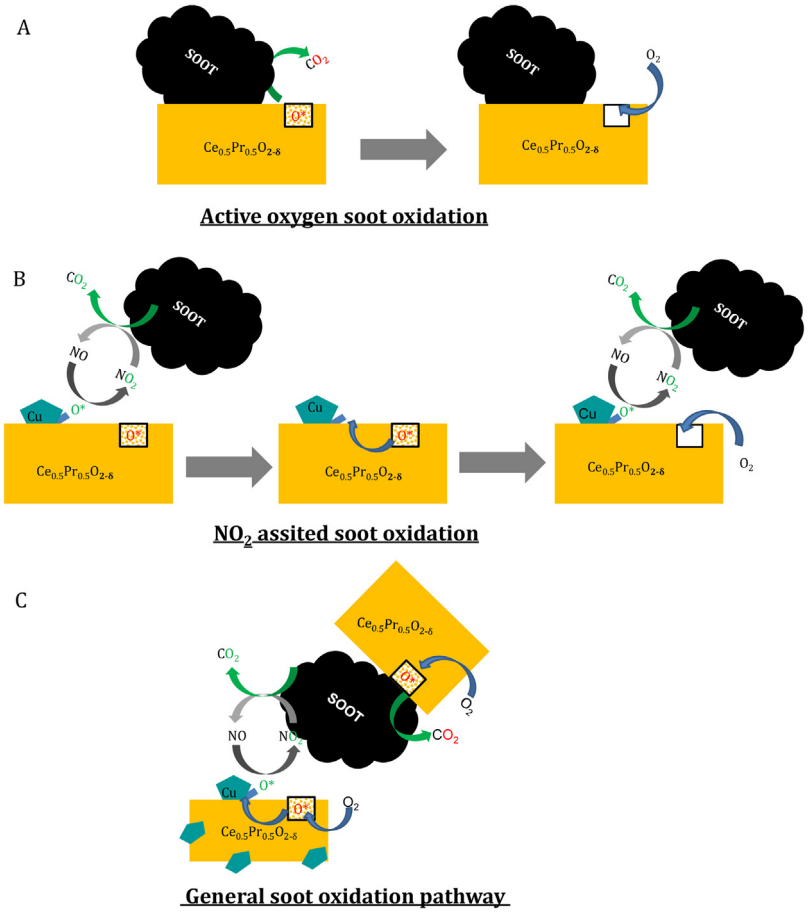

Fig. 7. (A) Active oxygen mechanism, (B) NO_2-assisted mechanisms, (C) overall mechanism of reaction for soot combustion over CuCePr + CePr catalysts.

tact with the catalyst takes the active oxygen from the catalyst surface promoting oxidation and creating new vacancies, which are quickly filled by the gas phase or subsurface oxygen. This mechanism depends on the catalyst-soot contact points/surfaces that are maximized by evaluating the catalyst performances under tight contact mode. The experiments performed in O_2/N_2 under tight contact conditions evidenced no difference among the various xCuCePr + yCePr catalysts, regardless to the amount of copper. Only the active oxygen mechanism is operative under these reaction conditions and the presence of copper does not affect the capacity of ceria-praseodymia to provide oxygen for the combustion of soot.

Fig. 7B describes the so-called NO_x-assisted mechanism, which is operative in the presence of NO. Under these conditions, oxidation of NO to NO_2 is initiated at the Cu O-$Ce_{0.5}Pr_{0.5}O_{2-\delta}$ interface with CuO effectively adsorbing NO, and with $Ce_{0.5}Pr_{0.5}O_{2-\delta}$ on the interface serving as source of oxygen to yield NO_2 [54], which then oxidizes soot. The reoxidation of the Cu O-$Ce_{0.5}Pr_{0.5}O_{2-\delta}$ interface is carried out by oxygen from the $Ce_{0.5}Pr_{0.5}O_{2-\delta}$ support, and the generated vacancies must be filled by gas phase O_2. The key role of copper in NO_2 production is evidenced by the linear relationship observed in NO oxidation to NO_2 (Fig. 4B). Therefore a relationship between copper content, NO_2 production and soot combustion should have been expected if the NO_x-assisted mechanism was the main reaction path in experiments performed under $NO_x/O_2/N_2$. However, this is in contrast to what reported in Fig. 5, likely because both the active oxygen and the NO_x assisted mechanisms are not independent and operate in close cooperation.

The active oxygen and the NO_x-assisted soot combustion mechanisms have different features. Active oxygen is expected to be more oxidizing than NO_2 but the lifetime of active oxygen is much shorter. Hence, soot combustion by active oxygen is very efficient but is limited to the few contact points existing between soot and catalyst particles mixed in loose contact. On the contrary, NO_2 can travel from the catalyst to soot without restrictions, but is less oxidizing than active oxygen.

When copper is loaded on $Ce_{0.5}Pr_{0.5}O_{2-\delta}$, the production of active oxygen is favoured because copper improves the catalyst reduction, as deduced from H_2-TPR experiments (Fig. 3A), and this active oxygen production is mainly located at the Cu O-$Ce_{0.5}Pr_{0.5}O_{2-\delta}$ interface. During the course of the soot combustion reactions performed in the presence of NO_x, this active oxygen produced at the Cu O-$Ce_{0.5}Pr_{0.5}O_{2-\delta}$ interface could potentially react with either NO, to yield NO_2, or with soot. The reaction with soot has less chance to occur compared to NO, due to the immobility of soot in the solid phase. Therefore, the improved production of active oxygen at the Cu O-$Ce_{0.5}Pr_{0.5}O_{2-\delta}$ interface mainly benefits the NO_x-assisted mechanism. However, the positive effect of copper improving NO_2 production has a penalty in the active oxygen mechanism, because it creates a lack of oxygen on $Ce_{0.5}Pr_{0.5}O_{2-\delta}$. If catalyst oxygen is consumed at the Cu O-$Ce_{0.5}Pr_{0.5}O_{2-\delta}$ interface mainly in NO_2 formation, the $Ce_{0.5}Pr_{0.5}O_{2-\delta}$ support transfers its oxygen to the Cu O-$Ce_{0.5}Pr_{0.5}O_{2-\delta}$ interface to compensate the oxygen imbalance. Therefore, there is less oxygen on $Ce_{0.5}Pr_{0.5}O_{2-\delta}$ available to be transferred directly to soot; that is, the active oxygen mechanism is affected negatively.

It is important to pay attention to the geometrical picture of a CuCePr-soot loose contact mixture during the catalytic combustion in $NO_x/O_2/N_2$. Since the amount of copper on the CuCePr catalyst is small with regard to $Ce_{0.5}Pr_{0.5}O_{2-\delta}$, it is more likely

that soot is in contact with the $Ce_{0.5}Pr_{0.5}O_{2-\delta}$ support than with the Cu O-$Ce_{0.5}Pr_{0.5}O_{2-\delta}$ interface, that is, in a CuCePr-soot loose contact mixture, statistically, there will be much more soot-$Ce_{0.5}Pr_{0.5}O_{2-\delta}$ contact points that soot-Cu O-$Ce_{0.5}Pr_{0.5}O_{2-\delta}$ contact points. As mentioned, copper promotes the reducibility at the Cu O-$Ce_{0.5}Pr_{0.5}O_{2-\delta}$ interface and this locates the most reactive oxygen species in that interface and creates a shortage of oxygen on the $Ce_{0.5}Pr_{0.5}O_{2-\delta}$ support. NO can move freely and pick active oxygen at the Cu O-$Ce_{0.5}Pr_{0.5}O_{2-\delta}$ interface, but soot must react with the oxygen available at the soot-catalyst contact points. Therefore the presence of copper hinders the active oxygen mechanism because most soot-catalyst contact points are not at the Cu O-$Ce_{0.5}Pr_{0.5}O_{2-\delta}$ interface but are with the $Ce_{0.5}Pr_{0.5}O_{2-\delta}$ support that suffers from a shortage of oxygen.

The penalty that the NO_2-assisted mechanism produces in the active oxygen mechanism can be partially avoided mixing $Ce_{0.5}Pr_{0.5}O_{2-\delta}$ particles with and without copper, and the results compiled in Fig. 5 suggest that the optimum composition is obtained with a mixture of 40% Cu/$Ce_{0.5}Pr_{0.5}O_{2-\delta}$ and 60% $Ce_{0.5}Pr_{0.5}O_{2-\delta}$. The main role of the Cu/$Ce_{0.5}Pr_{0.5}O_{2-\delta}$ particles is to accelerate the oxidation of NO to NO_2, promoting the NO_x-assisted soot combustion, but without affecting the active oxygen mechanism taking place on the remaining 60% of copper-free $Ce_{0.5}Pr_{0.5}O_{2-\delta}$ particles.

The benefit of mixing $Ce_{0.5}Pr_{0.5}O_{2-\delta}$ particles with and without copper in a single catalyst formulation is evidenced by comparing the performance of (2%)CuCePr and 40CuCePr + 60CePr. Both catalysts have the same amount of copper, but in the former copper is loaded in the whole $Ce_{0.5}Pr_{0.5}O_{2-\delta}$ support while in the latter the same amount of copper is loaded only on 40% of the $Ce_{0.5}Pr_{0.5}O_{2-\delta}$ particles. The H_2-TPR experiments (Fig. 3B) show that (2%)CuCePr is reduced in a single step, that is, the high reducibility of the Cu O-$Ce_{0.5}Pr_{0.5}O_{2-\delta}$ system prevails. On the contrary, the reduction profile of 40CuCePr + 60CePr shows two reduction events that could be related to the presence of two types of active sites during the soot combustion experiments. The most easily reduced sites located on copper-containing $Ce_{0.5}Pr_{0.5}O_{2-\delta}$ particles mainly promote NO oxidation to NO_2, and the sites reduced at higher temperatures located on copper-free $Ce_{0.5}Pr_{0.5}O_{2-\delta}$ particles mainly contribute to the active oxygen mechanism.

5. Conclusions

5%Cu/$Ce_{0.5}Pr_{0.5}O_{2-\delta}$ and $Ce_{0.5}Pr_{0.5}O_{2-\delta}$ oxides have been prepared and mixed in different ratios, and the resulting catalysts have been characterized and tested for soot combustion. The optimum catalyst for soot combustion (in loose contact) with $NO_x/O_2/N_2$ is the mixture containing 40%wt. Cu/$Ce_{0.5}Pr_{0.5}O_{2-\delta}$ and 60%wt. $Ce_{0.5}Pr_{0.5}O_{2-\delta}$. This mixture, that combines $Ce_{0.5}Pr_{0.5}O_{2-\delta}$ particles with and without copper, is more active than a reference catalyst with the same amount of copper, but distributed in the whole Ce-Pr mixed oxide support.

The benefit of mixing $Ce_{0.5}Pr_{0.5}O_{2-\delta}$ particles with and without copper in a single catalyst is that the participation of the two soot combustion mechanisms based on active oxygen and NO_2, is optimized. The catalyst that combines $Ce_{0.5}Pr_{0.5}O_{2-\delta}$ particles with and without copper has two different types of active sites, where the two soot combustion mechanisms take place. The particles with copper mainly promote the catalytic oxidation of NO to NO_2 (the NO_x-assisted mechanism) while those without copper are more effective promoting the active oxygen mechanism. If copper is loaded homogeneously in all the $Ce_{0.5}Pr_{0.5}O_{2-\delta}$ particles, the positive effect of copper in improving NO_2 is offset by the penalty in the active oxygen mechanism, and the overall performance of the catalyst in soot combustion is lower.

Acknowledgments

The authors thank financial support from MIUR (Futuro in ricerca, FIRB 2012, project SOLYST), Regione Autonoma Friuli Venezia Giulia, Generalitat Valenciana (Project PROMETEOII/2014/010), Spanish Ministry of Economy and Competitiveness (Project CTQ2012-30703) and UE (FEDER funding).

References

[1] B.A.A.L. van Setten, M. Makkee, J.A. Moulijn, Catal. Rev. Sci. Eng. 43 (2001) 489–564.
[2] W.A. Majewski, M.K. Khair, Diesel Emissions and Their Control, SAE, International, Warrendale PA, USA, 2006.
[3] D. Fino, Sci. Technol. Adv. Mat. 8 (2007) 93–100.
[4] M.V. Twigg, Appl. Catal. B: Environ. 70 (2007) 2–15.
[5] A.M. Hernandez-Gimenez, D.L. Castello, A. Bueno-Lopez, Chem. Papers 68 (2014) 1154–1168.
[6] A. Trovarelli, C. deLeitenburg, G. Dolcetti, Chem. Tech. 27 (1997) 32–37.
[7] A. Laachir, V. Perrichon, A. Badri, J. Lamotte, E. Catherine, J.C. Lavalley, J. Elfallah, L. Hilaire, F. Lenormand, E. Quemere, G.N. Sauvion, O. Touret, J. Chem. Soc. Faraday T. 87 (1991) 1601–1609.
[9] S. Bensaid, N. Russo, D. Fino, Catal. Today 216 (2013) 57–63.
[10] M. Piumetti, S. Bensaid, N. Russo, D. Fino, Appl. Catal. B: Environ. 165 (2015) 742–751.
[11] E. Aneggi, D. Wiater, C. de Leitenburg, J. Llorca, A. Trovarelli, ACS Catal. 4 (2014) 172–181.
[12] A. Trovarelli, Catal. Rev. Sci. Eng. 38 (1996) 439–520.
[13] P. Fornasiero, G. Balducci, R. DiMonte, J. Kaspar, V. Sergo, G. Gubitosa, A. Ferrero, M. Graziani, J. Catal. 164 (1996) 173–183.
[14] R. Di Monte, J. Kaspar, J. Mater. Chem. 15 (2005) 633–648.
[15] B.M. Reddy, A. Khan, Y. Yamada, T. Kobayashi, S. Loridant, J.C. Volta, J. Phys. Chem. B 107 (2003) 11475–11484.
[16] A. Trovarelli, Comments Inorg. Chem. 20 (1999) 263–284.
[17] J. Kaspar, P. Fornasiero, M. Graziani, Catal. Today 50 (1999) 285–298.
[18] A. Bueno-Lopez, K. Krishna, M. Makkee, J.A. Moulijn, J. Catal. 230 (2005) 237–248.
[19] E. Aneggi, M. Boaro, C. de Leitenburg, G. Dolcetti, A. Trovarelli, Catal. Today 112 (2006) 94–98.
[20] E. Aneggi, M. Boaro, C. de Leitenburg, G. Dolcetti, A. Trovarelli, J. Alloy Compd. 408 (2006) 1096–1102.
[21] E. Aneggi, C. de Leitenburg, A. Trovarelli, Catal. Today 181 (2012) 108–115.
[22] E. Aneggi, C. de Leitenburg, J. Llorca, A. Trovarelli, Catal. Today 197 (2012) 119–126.
[23] N. Guillen-Hurtado, A. Garcia-Garcia, A. Bueno-Lopez, Appl. Catal. B: Environ. 174 (2015) 60–66.
[24] K. Krishna, A. Bueno-Lopez, M. Makkee, J.A. Moulijn, Top. Catal. 42–43 (2007) 221–228.
[25] P. Fang, M.F. Luo, J.Q. Lu, S.Q. Cen, X.Y. Yan, X.X. Wang, Thermochim. Acta 478 (2008) 45–50.
[26] V.R. Perez, A. Bueno-Lopez, Chem. Eng. J. 279 (2015) 79–85.
[27] A. Bueno-Lopez, Appl. Catal. B: Environ. 146 (2014) 1–11.
[28] M. Machida, Y. Murata, K. Kishikawa, D.J. Zhang, K. Ikeue, Chem. Mater. 20 (2008) 4489–4494.
[29] M.S. Gross, M.A. Ulla, C.A. Querini, J. Molec. Catal. A 352 (2012) 86–94.
[30] X.D. Wu, F. Lin, H.B. Xu, D. Weng, Appl. Catal. B: Environ. 96 (2010) 101–109.
[31] K. Tikhomirov, O. Krocher, M. Elsener, A. Wokaun, Appl. Catal. B: Environ. 64 (2006) 72–78.
[32] D.A. Weng, J. Li, X.D. Wu, Z.C. Si, J. Environ. Sci.—China 23 (2011) 145–150.
[33] X.D. Wu, Q. Liang, D. Weng, Z.X. Lu, Catal. Commun. 8 (2007) 2110–2114.
[34] I. Atribak, B. Azambre, A.B. Lopez, A. Garcia-Garcia, Appl. Catal. B: Environ. 92 (2009) 126–137.
[35] A. Setiabudi, J.L. Chen, G. Mul, M. Makkee, J.A. Moulijn, Appl. Catal. B: Environ. 51 (2004) 9–19.
[36] B.J. Cooper, S.A. Roth, Platinum Metals Rev. 35 (1991) 178–187.
[37] J. Gimenez-Manogil, A. Bueno-Lopez, A. Garcia-Garcia, Appl. Catal. B: Environ. 152 (2014) 99–107.
[38] E. Aneggi, C. de Leitenburg, G. Dolcetti, A. Trovarelli, Catal. Today 114 (2006) 40–47.
[39] A. Setiabudi, J. Chen, G. Mul, M. Makkee, J.A. Moulijn, Appl. Catal. B: Environ. 51 (2004) 9–19.
[40] R. Jenkins, R. Snyder, Introduction to X-ray Powder Diffractometry, Wiley, New York, 1996.
[41] R.A. Young, The Rietveld Method IUCr Oxford, University Press, New York, 1993.
[42] A.C. Larson, R.B.V. Dreele, General Structure Analysis System GSAS, Los Alamos National Laboratory, 2016, pp. 2000.
[43] B.H. Toby, J. Appl. Crystallogr. 34 (2001) 210–213.
[44] A.R. West, Solid State Chemistry and Its Applications, John Wiley and Sons, New York, 1995.
[45] D.J. Kim, J. Am. Ceram. Soc. 72 (1989) 1415–1421.
[46] F. Lin, X.D. Wu, D. Weng, Catal. Today 175 (2011) 124–132.
[47] V.G. Keramidas, W.B. White, J. Chem. Phys. 59 (1973) 1561–1562.

[48] M.F. Luo, Z.L. Yan, L.Y. Jin, J. Mol. Catal. A 260 (2006) 157–162.
[49] J.R. Mcbride, K.C. Hass, B.D. Poindexter, W.H. Weber, J. Appl. Phys. 76 (1994) 2435–2441.
[50] G.Q. Xie, M.F. Luo, M. He, P. Fang, J.M. Ma, Y.F. Ying, Z.L. Yan, J. Nanopart. Res. 9 (2007) 471–478.
[51] A.D. Logan, M. Shelef, J. Mater. Res. 9 (1994) 468–475.
[52] E. Poggio-Fraccari, F. Marino, M. Laborde, G. Baronetti, Appl. Catal. A: Gen. 460 (2013) 15–20.
[53] B. de Rivas, N. Guillen-Hurtado, R. Lopez-Fonseca, F. Coloma-Pascual, A. Garcia-Garcia, J.I. Gutierrez-Ortiz, A. Bueno-Lopez, Appl. Catal. B: Environ. 121 (2012) 162–170.
[54] X.L. Tang, B.C. Zhang, Y. Li, Y.D. Xu, Q. Xin, W.J. Shen, Appl. Catal. A: Gen. 288 (2005) 116–125.
[55] A. Martinez-Arias, A.B. Hungria, G. Munuera, D. Gamarra, Appl. Catal. B: Environ. 65 (2006) 207–216.
[56] A. Arango-Diaz, J.A. Cecilia, E. Moretti, A. Talon, P. Nunez, J. Marrero-Jerez, J. Jimenez-Jimenez, A. Jimenez-Lopez, E. Rodriguez-Castellon, Int. J. Hydrogen Energy 39 (2014) 4102–4108.
[57] J.A. Cecilia, A. Arango-Diaz, V. Rico-Perez, A. Bueno-Lopez, E. Rodriguez-Castellon, Catal. Today 253 (2015) 115–125.
[58] H. Muroyama, S. Hano, T. Matsui, K. Eguchi, Catal. Today 153 (2010) 133–135.